Journal of Solid Mechanics Vol. 11, No. 1 (2019) pp. 60-77
DOI: 10.22034/JSM.2019.664217

Numerical Analysis of Composite Beams Under Impact by a Rigid Particle

N. Akbari [1,*], B. Chabsang [2]

[1]*Department of Aerospace Engineering, Shahid Sattari Aeronautical University of Science Technology, Tehran, Iran*
[2]*Departmen of Mechanical Engineering, Amirkabir University of Technology, Tehran, Iran*

Received 10 September 2018; accepted 10 December 2018

ABSTRACT

Analysis of a laminated composite beam under impact by a rigid particle is investigated. The importance of this project is to simulate the impact of objects on small scale aerial structures. The stresses are considered uni-axial bending with no torsion loading. The first order shear deformation theory is used to simulate the beam. After obtaining kinematic and potential energy for a laminated composite beam, the motion equations, boundary conditions and initial conditions are obtained by using Hamilton's principle. The deformation of beam is considered large so these equations are nonlinear. Then by using the numerical methods such as generalize differential quadrature (GDQ) and Newmark methods, the equations will be converted in to a set of nonlinear algebraic equations. These nonlinear equations are solved by numerical methods such as Newton- Raphson. By solving the equations, the displacement of beam and rotation of cross section in terms of time for different number of points of beam for variety of orientation angle of layers are obtained. Then the displacements of impacted point of beam, stresses and contact forces in different times for variety of orientation of layers for different situations of impact are compared.

Keywords: Composite beam; Impact; Rigid mass; Large deformation.

1 INTRODUCTION

COMPOSITE materials are widely used in various industries such as aerospace, auto motives, ship buildings and other industries. So far, many studies have been carried out to analyze composite beams and sheets under various loading conditions, including impact loads. One of the most important models used to study the behavior of structures under impact is Hertz contact law which is based on the mass and spring model with two degrees of freedom. This law was first introduced by Hertz [1]. In this model, Hertz has studied the mechanical impact of spherical bodies (with radius d). These objects interact with each other in a circle area with radius dk ($dk > d$) and each other imposes a limited pressure. Another model that used to study the behavior of structures under impact is the Zener model [2]. This model is used to study impact of a particle on a thin sheet, assuming that input kinetic energy is divided into two stresses, one remains in the impact zone and the other spreads along the sheet. Contrary to

*Corresponding author. Tel.: +98 2164002217.
E-mail address: nozar@ssau.ac.ir (N. Akbari).

the Hertz contact Law, which has no energy dissipation, in this model, some of the kinetic energy that is transmitted along the thin sheet is wasted. Müller et al. [3] studied the impact of steel spherical balls on thin sheets. The model used in this work was the Zener model. They also measured the collision time by an experimental test. According to this test, the contact time has an inverse relationship with thickness of the plate and has a direct relation with the size of spherical balls. Many studies can be referred in the field of calculation of energy dissipation during the impact. Boettcher et al. [4] studied the energy of a thick plate at high impact speeds by using the modified Zener's model. In this work, the longitudinal and transverse wave stresses published on the sheet have a significant effect on the energy dissipation. Hunter developed an analytical relationship to calculate the energy consumed during an impact with the approximations used in the Hertz model [5]. Although the relation obtained from his work was very different from the results obtained from the Hertz relationship. Reed [6] also presented a modified model for calculating waste energy. The model presented by him predicts energy waste about 4.5 times more than Hunter's relationship, and is more accurate than the experimental results. Weir and Tallon [7] examined behavior of elastic-plastic impact. They considered the coefficient of restitution as a function of relative velocity ratio and velocity of stress waves. They also concluded that the coefficient of restitution of two spherical bodies was 19% less than the collision of a spherical object with a smooth surface.

In the field of impact on beams, the work of Kelly can be referred [8]. He examined the impact of a mass on an infinite beam to improve the design of the carriageways at highways in an analytical work. He used Euler-Bernoulli and Timoshenko models for beam modeling in this project. Sun and Huang [9] studied the elastic and plastic impact of a particle on a beam. They considered the transverse deformation of beam as a 5 order polynomial and solved the problem by finite element methods. Yufeng et al. [10] studied the elastic collision of a mass on a beam with different boundary conditions. They examined the propagation of longitudinal and transverse tensile waves in the beam and the effect of boundary conditions on the reflected waves. The model that they used for the beam is Timoshenko's beam model. Kiani et al. [11] also provided a model for impact on FGM beams. The contact stiffness of this model is a function of the ceramic and metal phases in the beam. In the field of impact on column, the work of Rezvanian et al can be referred [12]. They used GDQ method and Newmark method in order to solve the problem numerically. Also the work of Samani et al can be mentioned [13]. They analyze impact on composite columns, having initial geometric imperfection by rigid particle. In the field of impact on composite materials the work of Singh and Mahajan can be referred [14]. They studied the impact on composite sheets using a mass and spring model. Also the work of Shivakumar et al. can be pointed [15]. In this article, they studied impact on graphite-epoxy circular sheets. In this field, we can mention the work of Lam and Sathiyamoorthy [16] who studied the impact of several particles on a composite beam. The contact force in this work is based on the Hertz Contact law.

In this paper, a numerical approach to the impact of a rigid particle on a cantilevered beam is discussed. This impact is considered elastic. Examples of these impacts can be seen in the collision of small stones or objects on the wing of the plane, helicopter blade and other structures of the air. In these structures, the choice of materials for the improvement of design and the quality of structures is very important; therefore, in this project, a numerical study of the behavior of graphite / epoxy composite beams in the face of impact is considered. Due to its high strength and low weight, these materials are great use in the construction of air structures. Also, the effective of parameters are examined. In the following, a comparison is made between the behavior of aluminum beams (including materials used in building aircraft bodies) and graphite-epoxy beams due to the impact of a rigid particle. Because the size of particle is very small, unlike previous works, the contact force between the particle and the beam is considered as a point at the point of impact, and the pressure which is considered in Hertz contact law around area of impact which should be obtained by experimental tests is neglected. One of the innovations of this work is to simulate the oblique impact on the free- head of beam without considering hertz pressure. Due to the fact that the deformations of the beam can be large, the equations are obtained nonlinearly. Initially, the relation between kinetic energy and potential energy for a composite beam is obtained, assuming that the stresses are one dimensional. Then, using the Hamilton principle, the relations of motion and boundary conditions are also derived. In the following, numerical methods are used to solve equations for a graphite/ epoxy composite beam.

2 THEORETICAL FORMULATION

Motion equations are obtained by Hamilton's principle. The cantilever beam is straight and the particle hits on free head of beam. This particle is considered rigid, so the kinetic and gravity potential energy is considered and strain energy is neglected. Fig. 1 shows the geometry of the beam and the particle. The x- axis is considered as base axis of orientation of composite layers.

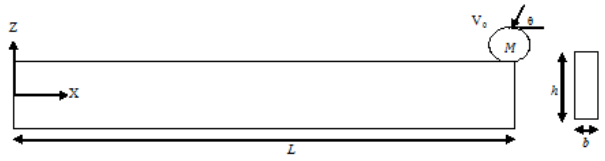

Fig.1
Schematic of impact on beam by a rigid particle.

The displacement of beam is written based on Timoshenko's beam model. Therefore, the displacement relations of the beam are considered as follows.

$$u_x(x,z,t) = u(x,t) + z\,\varphi(x,t) \tag{1a}$$

$$u_y(x,z,t) = 0 \tag{1b}$$

$$u_z(x,z,t) = w(x,t) \tag{1c}$$

where in Eq. (1) u_x , u_y , u_z are the components of beam displacement in direction of *x,y* and *z* respectively. Also *u* and *w* are the displacement of middle surface of beam in direction of *x, z* and φ is rotation of middle surface about y axis. The strain-displacement relations are considered as follows with regard to Van Karman's theory. The deformation of beam is considered large so in this paper based on Von- Karman's theory, the strains are considered nonlinear [17].

$$\varepsilon_{xx} = \frac{\partial u_x}{\partial x} + \frac{1}{2}\left(\frac{\partial u_z}{\partial x}\right)^2 \tag{2a}$$

$$\gamma_{xz} = \frac{\partial u_x}{\partial z} + \frac{\partial u_z}{\partial x} \tag{2b}$$

For an orthotropic beam the stress- strain relations are written as follows according to [18].

$$\sigma_{xx} = C_{11}\varepsilon_{xx} \ , \ \tau_{xz} = C_{55}\gamma_{xz} \tag{3}$$

In these relations C_{11} and C_{55} are obtained from following equations.

$$C_{11} = \overline{C}_{11} - \frac{\overline{C}_{12}\overline{C}_{12}}{\overline{C}_{22}} \ , \ C_{55} = \overline{C}_{55} \tag{4}$$

In Eq. (4) $\overline{C}_{ij}$ is transformed elastic coefficient for orthotropic materials. These coefficients are a function of the angle between the principle orientation of layers and the *x*-axis. Their values are obtained from [19]. The Hamilton's principle relation is written as follows:

$$\int_{t_1}^{t_2} \delta(T - U)\,dt = 0 \tag{5}$$

where in Eq. (5), *T* is the kinetic energy of the beam and particle, and *U* is the potential energy of the beam and particle, which is defined as follows.

$$U = \pi - W_p \tag{6}$$

In all previous projects, when the impact on a structure is investigated, the contact force between the object and the beam is applied into a circular area with a specified radius. This contact force is function of radius of object, the properties of beam and object which are usually obtained experimentally. But in this paper, the dimension of particle impacted on beam is neglected, so that the contact force between beam and particle is applied on a point. This particle is attached to the beam during impact with the beam and is not detached until the contact force between the particle and the beam is zero. For this reason, we can consider the beam and particle collection as a single system. So in Hamilton's principle, the kinetic energy and potential energy of beam and particle are written together.

In the Eq. (6), π is the strain energy and W_p is the work of external forces which is the gravity of rigid particle in this article. The kinetic energy relation of the beam and the particle is as follows.

$$T = \frac{\rho b}{2}\int_0^L\int_{-\frac{h}{2}}^{\frac{h}{2}}\left[\dot{u}_x\left(x,z,t\right)^2+\dot{u}_z\left(x,z,t\right)^2\right]dzdx+\frac{1}{2}M\dot{u}_x\left(L,\frac{h}{2},t\right)^2+\frac{1}{2}M\dot{u}_z\left(L,\frac{h}{2},t\right)^2 \tag{7}$$

where in Eq. (7) ρ , b , L , h and M are density of beam, width of beam ,length of beam, thickness of beam and mass of particle respectively. The kinetic relation based on components of displacement is written as follows:

$$T = \frac{\rho b}{2}\int_0^L\int_{-\frac{h}{2}}^{\frac{h}{2}}\left[\left(\dot{u}\left(x,t\right)+z\,\dot{\varphi}\left(x,t\right)\right)^2+\dot{w}\left(x,t\right)^2\right]dzdx+\frac{1}{2}M\left[\dot{u}\left(L,t\right)^2+\dot{w}\left(L,t\right)^2+h\dot{u}\left(L,t\right)\dot{\varphi}\left(L,t\right)+\frac{1}{4}h^2\dot{\varphi}\left(L,t\right)^2\right] \tag{8}$$

The potential energy for the set of the beam and particle is written as follows:

$$U = b\int_0^L\int_{-\frac{h}{2}}^{\frac{h}{2}}\left(\frac{1}{2}\sigma_x\,\varepsilon_x+\frac{1}{2}k\,\tau_{xz}\,\gamma_{xz}\right)dzdx+Mgu_z\left(L,\frac{h}{2},t\right) \tag{9}$$

The coefficient of k is shear correction coefficient and its value is 5/6. In order to remove the stress and strain terms in Eq. (8), we use Eq. (2), (3) and (4). Thus, Eq. (8) is written in terms of the displacement components of the middle surface of the beam as follows.

$$U = \frac{b}{2}\int_0^L\int_{-\frac{h}{2}}^{\frac{h}{2}}\left[C_{55}k\left(\varphi+\frac{\partial w}{\partial x}\right)^2+C_{11}\left(\frac{\partial u}{\partial x}+\frac{1}{2}\left(\frac{\partial w}{\partial x}\right)^2+z\,\frac{\partial \varphi}{\partial x}\right)^2\right]dzdx+mgw\left(L,t\right) \tag{10}$$

By placing the Eq. (8) and (10) in Eq. (5), the motion equations are obtained as follows (the description of equations is written in appendix):

$$A_{11}\left(\frac{\partial^2 u}{\partial x^2}+\frac{\partial w}{\partial x}\frac{\partial^2 w}{\partial x^2}\right)+B_{11}\frac{\partial^2 \varphi}{\partial x^2}=\rho h\frac{\partial^2 u}{\partial t^2} \tag{11a}$$

$$D_{11}\frac{\partial^2 \varphi}{\partial x^2}+B_{11}\left(\frac{\partial^2 u}{\partial x^2}+\frac{\partial w}{\partial x}\frac{\partial^2 w}{\partial x^2}\right)-A_{55}k\left(\varphi+\frac{\partial w}{\partial x}\right)=\frac{1}{12}\rho h^3\frac{\partial^2 \varphi}{\partial t^2} \tag{11b}$$

$$A_{55}k\left(\frac{\partial \varphi}{\partial x}+\frac{\partial^2 w}{\partial x^2}\right)+B_{11}\left(\frac{\partial^2 \varphi}{\partial x^2}\frac{\partial w}{\partial x}+\frac{\partial \varphi}{\partial x}\frac{\partial^2 w}{\partial x^2}\right)+A_{11}\left(\frac{\partial^2 u}{\partial x^2}\frac{\partial w}{\partial x}+\frac{\partial u}{\partial x}\frac{\partial^2 w}{\partial x^2}+\frac{3}{2}\frac{\partial^2 w}{\partial x^2}\left(\frac{\partial w}{\partial x}\right)^2\right)=\rho h\frac{\partial^2 w}{\partial t^2} \tag{11c}$$

The coefficients of A_{11}, A_{55}, B_{11} and D_{11} are obtained from following relations:

$$A_{11}=\sum_{k=1}^{m} C_{11k}\left(h_{k+1}-h_k\right) \tag{12a}$$

$$B_{11}=\frac{1}{2}\sum_{k=1}^{m} C_{11k}\left(h^2{}_{k+1}-h^2{}_k\right) \tag{12b}$$

$$D_{11}=\frac{1}{3}\sum_{k=1}^{m} C_{11k}\left(h^3{}_{k+1}-h^3{}_k\right) \tag{12c}$$

$$A_{55}=\sum_{k=1}^{m} C_{55k}\left(h_{k+1}-h_k\right) \tag{12d}$$

In Eq. (12), *m* is the number of layers of the laminated composite beam. For a cantilevered beam the boundary conditions are written as follows:

$$\begin{aligned} &x=0: \\ &u=\varphi=w=0 \end{aligned} \tag{13}$$

$$x=L:$$

$$A_{11}\left(\frac{\partial u}{\partial x}+\frac{1}{2}\left(\frac{\partial w}{\partial x}\right)^2\right)+B_{11}\frac{\partial \varphi}{\partial x}+\frac{M}{b}\left(\frac{\partial^2 u}{\partial t^2}+\frac{h}{2}\frac{\partial^2 \phi}{\partial t^2}\right)=0 \tag{14a}$$

$$D_{11}\frac{\partial \phi}{\partial x}+B_{11}\left(\frac{\partial u}{\partial x}+\frac{1}{2}\left(\frac{\partial w}{\partial x}\right)^2\right)+\frac{Mh}{2b}\left(\frac{\partial^2 u}{\partial t^2}+\frac{h}{2}\frac{\partial^2 \phi}{\partial t^2}\right)=0 \tag{14b}$$

$$A_{55}k\left(\phi+\frac{\partial w}{\partial x}\right)+A_{11}\left(\frac{\partial u}{\partial x}\frac{\partial w}{\partial x}+\frac{1}{2}\left(\frac{\partial w}{\partial x}\right)^3\right)+B_{11}\frac{\partial \varphi}{\partial x}\frac{\partial w}{\partial x}+\frac{M}{b}\left(g+\frac{\partial^2 w}{\partial t^2}\right)=0 \tag{14c}$$

The vertical contact force on the free head of beam ($x=L$) is as follows:

$$V=-bA_{55}k\left(\phi+\frac{\partial w}{\partial x}\right)-bA_{11}\left(\frac{\partial u}{\partial x}\frac{\partial w}{\partial x}+\frac{1}{2}\left(\frac{\partial w}{\partial x}\right)^3\right)-bB_{11}\frac{\partial \varphi}{\partial x}\frac{\partial w}{\partial x} \tag{15}$$

This force is equal to zero at the instant that the particle is separated from the beam. We consider the beam at *t=0* is in static equilibrium. Therefore, the initial conditions are as follows. V_0 is initial velocity.

$$u\left(x,0\right)=\varphi\left(x,0\right)=w\left(x,0\right)=\dot{u}\left(x,0\right)=\dot{\phi}\left(x,0\right)=0\ ,\ x\epsilon\left[0,L\right] \tag{16a}$$

$$\dot{w}\left(x,0\right)=0,\ x\epsilon\left[0,L\right) \tag{16b}$$

$$\dot{w}\left(x,0\right)=V_0,\ x=L \tag{16c}$$

3 NUMERICAL METHODS USED IN SOLVING EQUATIONS

Numerical methods are used to solve Eq. (11). To remove time derivatives and convert them into an algebraic relationship, Newmark method is used [20]. Their relations are written as follows:

$$\dot{X}^{(n+1)} = \dot{X}^{(n)} + (1-\gamma)\ddot{X}^{(n)}\Delta t + \gamma \ddot{X}^{(n+1)}\Delta t \tag{17a}$$

$$X^{(n+1)} = X^{(n)} + \dot{X}^{(n)}\Delta t + \left(\frac{1}{2} - \beta\right)\ddot{X}^{(n)}\Delta t^2 + \beta \ddot{X}^{(n+1)}\Delta t^2 \tag{17b}$$

In the Eq. (17), Δt is the time step, and γ and β are the irregular parameters on which the stability and damping of the system are controlled. When the time integral methods are used, there are some perturbations at the initial time of the analysis. These perturbations are generally such that the results are oscillating at the beginning of the analysis. These perturbations are caused by high frequency modes [21]. So the results obtained from time integration methods at initial times do not have enough accuracy. Of course in order to decrease these perturbations we can use methods that dissipate high frequency. In Newmark method, high frequency is controlled by γ and β coefficients.

In order to eliminate the derivatives relative to the place and convert it to an algebraic expression, the generalized differential quadrature method is used. According to this method, the derivation of any quantity relative to the place is written as follows [21].

$$\frac{d^n f(x_i)}{dx^n} = \sum_{j=1}^{N} c_{ij}^{(n)} f(x_j);\ i = 1,2,\ldots,N\ ;\ n = 2,3,\ldots,N-1 \tag{18}$$

The coefficients $c_{ij}^{(n)}$ are also obtained from the following equation.

$$c_{ij}^{(1)} = \frac{M(x_i)}{(x_i - x_j)M(x_j)}\ ;\ i,j = 1,2,\ldots,N\ ;\ i \neq j \tag{19a}$$

$$c_{ii}^{(1)} = -\sum_{j=1, j\neq i}^{N} c_{ij}^{(1)} \tag{19b}$$

$$c_{ij}^{(n)} = n\left(c_{ij}^{(1)} c_{ii}^{(n-1)} - \frac{c_{ij}^{(n-1)}}{x_i - x_j}\right)\ ;\ i,j = 1,2,\ldots,N \tag{19c}$$

$$c_{ii}^{(n)} = -\sum_{j=1, j\neq i}^{N} c_{ij}^{(n)}\ ;\ n > 1 \tag{19d}$$

The function $M(x_i)$ is also obtained from the following equation.

$$M(x_i) = \prod_{j=1, j\neq k}^{N} (x_i - x_j) \tag{20}$$

We use the following equation to determine the discrete points.

$$x_i = \frac{L}{2}\left[1-\cos\left(\frac{i-1}{N-1}\pi\right)\right] \; ; \; i = 1,2,\ldots,N \tag{21}$$

By placing the Eq. (17) to (21), in Eq. (11) to (13), the motion equations become a nonlinear algebraic equation system. The equations after applying GDQ and Newmark method are written in appendix. These nonlinear equations are numerically solvable. One of these numerical methods is the Newton-Raphson method. To use this we need to have an initial guess. In this article, the initial conditions are used as initial guesses for the Newton- Raphson method for the first time step. After that, the solutions obtained at each time step are used as the initial guess for the next step. When numerical methods such as GDQ and Newmark are used, in each time step, the value of Eq. (15) is checked. While the sign of this relation changes, this shows that the contact force between this time step and previous step is equal to zero. This method also is used in other papers such as [12] and [13].

4 RESULTS AND DISCUSSIONS

The Graffiti- Epoxy AS/3501-6 cantilevered beam is considered. This beam consists of four layers with angles [0/90/90/0], [45/-45/-45/45] and [50/30/30/50] relative to the longitudinal axis of the beam. Also, in a separate analysis, the single-layer beam 0° is considered. The dimensional and physical properties of the beam are given in Table 1. In Table 2., mechanical properties of graphite / epoxy AS/3501-6 materials are given. The time step (Δt) and the number of discrete points are chosen 1×10^{-4} sec and 51 respectively. The parameters γ and β are selected 1.5 and 1 respectively [22]. These equations are solved by MATLAB software.

Table 1
Dimensional and physical properties of beam.

Properties	Unit	Value
Length (L)	m	0.15
thickness (h)	m	0.015
Width (b)	m	0.025
Density (ρ)	kg/m^3	1389.23
Mass of particle (M)	kg	0.5
Initial velocity (V_0)	m/s	5
Angle impact (θ)	°	90

Table 2
Mechanical properties of graphite/ epoxy AS/3501-6.

Properties	Unit	Value
E_1	GPa	144.8
E_2	GPa	9.65
G_{23}	GPa	3.34
G_{13}	GPa	4.14
G_{12}	GPa	4.14
ν_{12}	…	0.3

4.1 Validation of results

ABAQUS software is used to verify the results. As no literature could be found on the impact on free head of a laminated cantilever beam, verification of obtained results is done by ABAQUS software. However some previous papers which are investigated the impact on various structures; verify the results by finite element softwares (such as [11], [12] and [13]). In order to simulate the problem in ABAQUS, a beam with 0.15m length, 0.015m thickness and 0.025m width is plotted in this software. This beam is a rectangle cube. For modeling the particle, a rigid sphere is used and the radius of the sphere is chosen 1mm. The density of the sphere is chosen in such a way that the mass is 0.5 kg. The initial velocity of sphere is selected 5 m/s. The properties of the beam are applied in properties module. The ordering of the layers of the composite beam for [0/90/90/0] is done in property module too. The type of step in step module is selected as Dynamic, Explicit and the time period is the time which is gained from numerical solution of motion equations. The type of interaction of the sphere and the beam is selected as surface to surface contact; and

the property of the interaction in normal direction is selected hard contact. The rigid body constraint is applied on sphere. In load module, the head of the beam which sphere is not on it; is fixed. The size of mesh in mesh module is selected 1mm and the hex element is applied on the beam. The geometry of simulation is shown in Fig. 2.

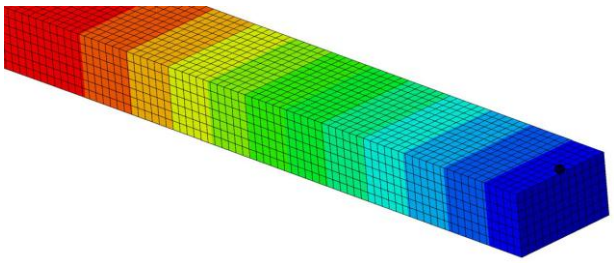

Fig.2
The geometry of simulation in ABAQUS.

In Table 3., the collision time for the composite beam is shown with the different orientation angles of layers. This time is obtained due to the removing of the vertical contact force found in Eq. (15).

Table 3
Contact time for laminated beam with different orientation angles of layers.

Orientation of layers	Impact time (s)
0°	0.002552653
[0/90/90/0]	0.002697777
[45/-45/45/-45]	0.008761795
[50/30/30/50]	0.009139955

In Fig. 3 and Fig. 4, the transverse displacement and contact force of 0° orthotropic beam in terms of time is shown. As shown in Fig. 3 and Fig. 4, the results obtained from the equations are approximately the same from the results obtained from the ABAQUS software. In Fig.5 and Fig. 6 the transverse displacement and contact force of [0/90/90/0] composite beam is shown. As shown in Fig. 5, the transverse displacement of four-layer beam with a direction [0/90/90/0] increases and the time of the collision is greater than the beam with a zero degree angle.

Also in Fig. 7, transverse displacement of 0°, [0/90/90/0], [45/-45/-45/45], [50/30/30/50] composite beam is shown. As shown in Fig. 7, the transverse displacement for the laminate beam with direction [50/30/30/50] is more than the laminate beam with directions [45/-45 /- 45/45], [0/90/90/0] and one-layer beam with angle 0°.

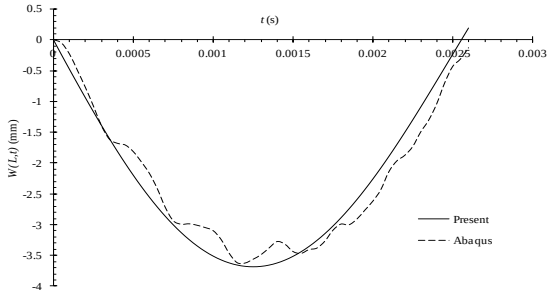

Fig.3
Transverse displacement of 0° composite beam.

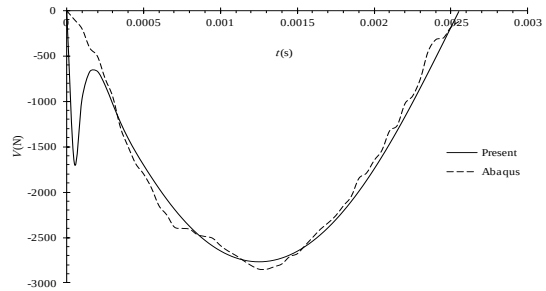

Fig.4
Contact force of 0° composite beam.

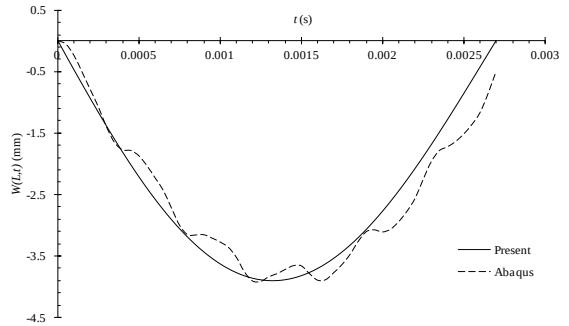

Fig.5
Transverse displacement of [0/90/90/0] composite beam.

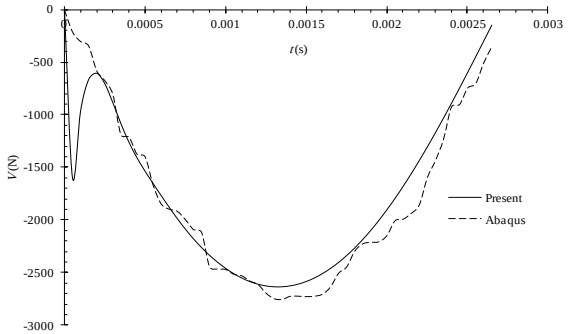

Fig.6
Contact force of [0/90/90/0] composite beam.

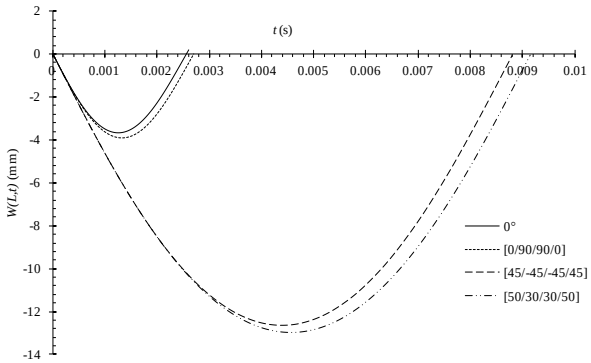

Fig.7
Transverse displacement of composite beam with under rigid particle.

4.2 Investigation of contact forces and stresses in the beam

In Fig. 8, the transverse contact force is shown in the impact point relative to time for a composite beam with different orientations. As shown in Fig. 8, when the principle axis is smaller relative the longitudinal axis of the beam, a greater contact force is generated in the beam and the beam has a greater flexural rigidity.

The fix head of the beam has the highest stress than the total beam. To illustrate the distribution of stress versus time, the normal stresses diagram at the fix head of beam is shown in Fig. 9.

The shear stress of the beam at the fix head of the beam relative to time is also shown in Fig. 10. As shown in Fig. 9 and 10, as the angles of the principle axis of the layers are longer relative to longitudinal axis of the beam, the normal and shear stresses in the beam are less. This feature can be used to design materials against fracture of impact. As shown in Fig. 8, Fig. 9 and Fig. 10, some results of the laminate beam fluctuate a lot. Oscillations of stresses in figures are due to interference of compressive and tensile stress waves. In this paper, there are longitudinal, bending and shear stress waves. So during impact of particle on the beam, these stress waves will distribute at beam with a certain velocity. So interference of these waves at a certain point leads to oscillate of stress diagrams. For [45/-45/-45/45] composite beam, these oscillating are more from others.

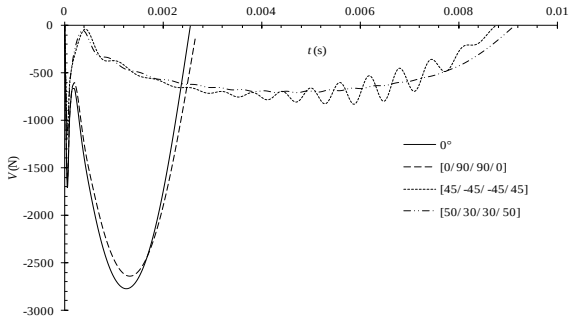

Fig.8
Contact force for laminated beam for different orientation angles of layers.

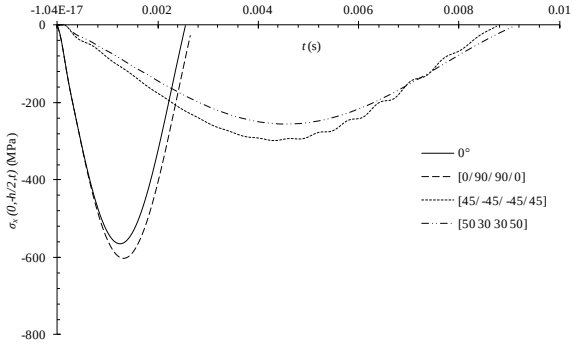

Fig.9
Normal stress at x=0, z=-h/2 for laminated beam for different orientation angles of layers.

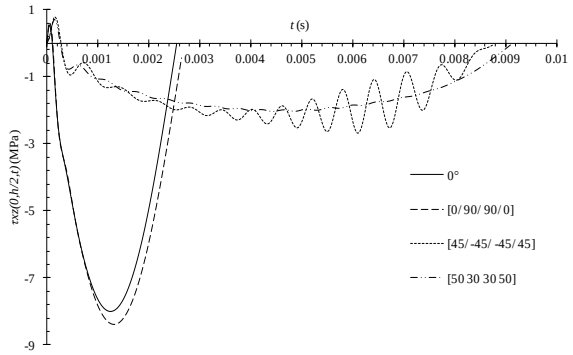

Fig.10
Shear stress at x=0, z=-h/2 for laminated beam for different orientation angles of layers.

4.3 Investigation of the effect of initial velocity of rigid particle

In order to examine the motion of the beam by impact of a rigid particle, a composite beam is considered with the angle of layer 0°. The initial velocities of the particle are 5, 6, 7 and 8 *m/s*. In Table 4., the separation time of a rigid particle from the beam for different initial velocities is shown. According to Table 4., it is evident that changing the initial velocity does not affect significantly on the amount of the collision time.

Table 4
Contact time for 0° laminated beam under the impact of a rigid particle with different initial velocities.

Initial velocity (*m/s*)	Contact time (*s*)
5	0.002552653
6	0.002570664
7	0.002592
8	0.0026168

In Fig. 11, the transverse displacement diagram of the beam is shown at the impact point of the beam for different initial velocity of particle. As shown in Fig. 11, due to the change in the initial velocity of the particle, the

transverse displacement of the beam increases, but the separation time of the particle from the beam is almost constant.

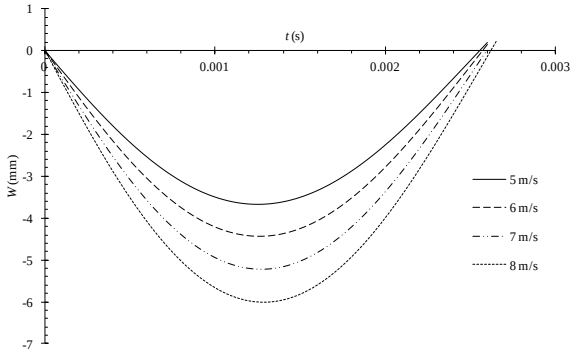

Fig.11
Transverse displacement of 0° composite beam under the impact of a rigid particle with different initial velocities.

4.4 Investigation of the effect of the mass of particle

In order to investigate the effect of the mass of the rigid particle on the impact, the beam is considered with the same previous properties. The angles of the principle axis of the layers are selected zero, and the mass of the rigid particle is 0.5, 1 and 1.5 *kg*. Fig. 12 shows the transverse displacement of the beam at the point of impact due to collision of a rigid particle with different masses. As shown in Fig. 12, as the mass of particle increases, the separated time and displacement of beam increases.

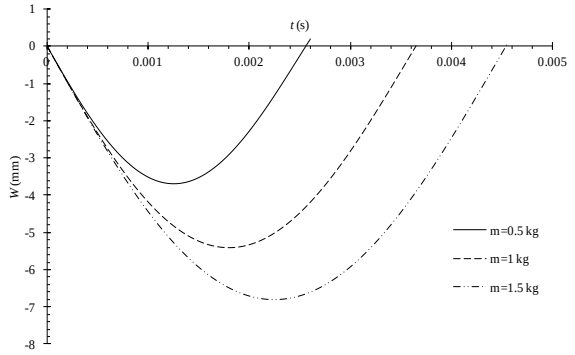

Fig.12
Transverse displacement of 0° composite beam under the impact of a rigid particle with different particle mass.

4.5 Comparison of impact on a composite and aluminum beam

Due to the lightness and high strength of aluminum, it has a great deal to make in the body of aircraft and helicopters. These materials have a high corrosion resistance compared to steel. But these materials have low resistance at high temperatures; they have little use in the construction of high-speed airborne structures. Airplane wings and helicopter blades are among those that are exposed to rigid bodies such as stones. In this section, a comparison is made between the behavior of the graphite-epoxy composite beams and the aluminum beams against impact for use in air constructions.

The motion equations for the aluminum beam are given in the appendix. The aluminum beam density is 2769 kg/m^3, the young's modulus is 68.9 *GPa*, and its Poisson coefficient is 0.25. In Fig. 13, the transverse displacement of the composite beams with the angles [0/ 90/0 90] and [45/-45/-45 /45] are compared with the aluminum beam. In Fig. 14 and 15, the normal and shear stresses of the beams are compared at fix head of beam.

As shown in Fig. 14 and 15, the aluminum beam has lower stresses than composite beam [0/90 90/0] and has more stresses than [45/-45/-45/45]. Therefore, determining the angle of the principle axis of the layers in composite materials can be effective in reducing the forces created in the structures.

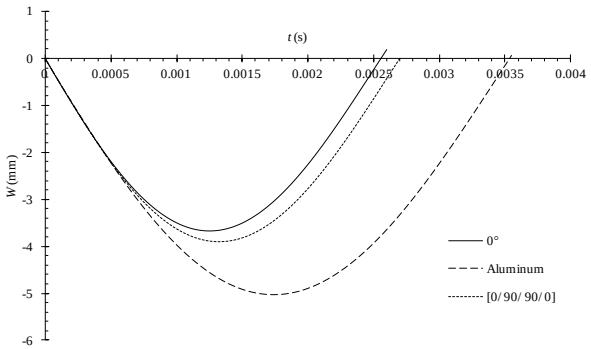

Fig.13
Transverse displacement of [0/ 90/ 90/ 0] and [45/ -45/ -45/ 45] composite beam and aluminum beam under the impact of a rigid particle.

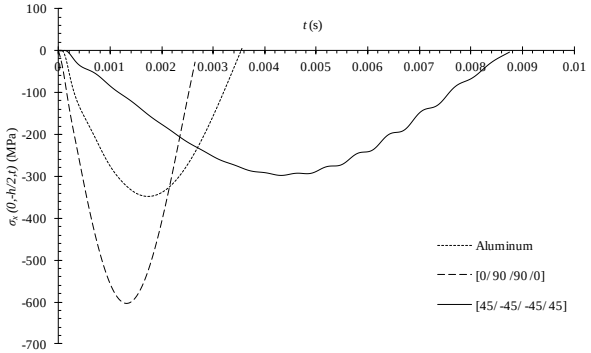

Fig.14
Normal stress at x=0, z=-h/2 for [0/ 90/ 90/ 0] and [45/ -45/ -45/ 45] composite beam and aluminum beam under the impact of a rigid particle.

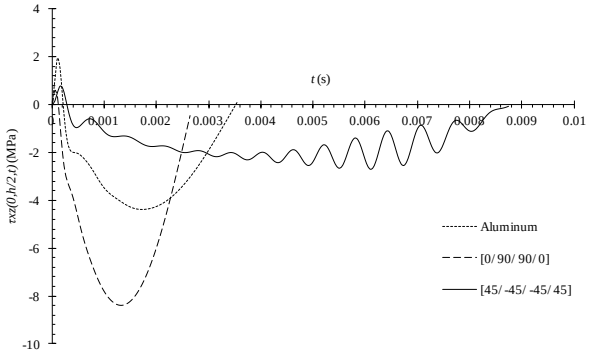

Fig.15
Shear stress at x=0, z=-h/2 for [0/ 90/ 90/ 0] and [45/ -45/ -45/45] composite beam and aluminum beam under the impact of a rigid particle.

4.6 Oblique impact on beam

In order to investigate the effect of the collision angle of the rigid particle with the beam, a zero-degree graphite composite beam with length of 0.3 m and thickness of 0.75×10^{-2} m are considered. The particle hits on the beam with an angle θ relative to the longitudinal axis. In this way, Eq. (16) is as follows:

$$u(x,0)=\varphi(x,0)=w(x,0)=\dot{\phi}(x,0)=0,\ \ x\epsilon[0,L] \tag{22a}$$

$$\dot{w}(x,0)=\dot{u}(x,0)=0,\ \ x\epsilon[0,L) \tag{22b}$$

$$\dot{w}(L,0)=V_0\sin(\theta),\ \ \dot{u}(L,0)=V_0\cos(\theta) \tag{22c}$$

In this case we consider the vertical contact force as separation criterion (Eq. (15)). In Fig. 16, the transverse displacement for the collision angles of 90, 60 and 45 degrees is shown.

As shown in Fig. 16 increasing the angle of impact relative to the horizontal axis (θ) increases the transverse displacement of the beam. This increase in displacement reduces the forces and tensions that arise in the beam. Therefore, when the particle is collided transversally, tensions and forces are in a more critical state. Also as shown in Fig. 16, the separation time increased by decreasing the angle of impact. One of the reasons is that, in each angle of impact, the input energy (the kinetic energy of particle at initial of impact) is equal together. But as the angle of impact decreases, the transverse velocity decreases and also the transverse contact force decreases, so because the initial energy is constant, as the angle of impact decreases, the separation time increases.

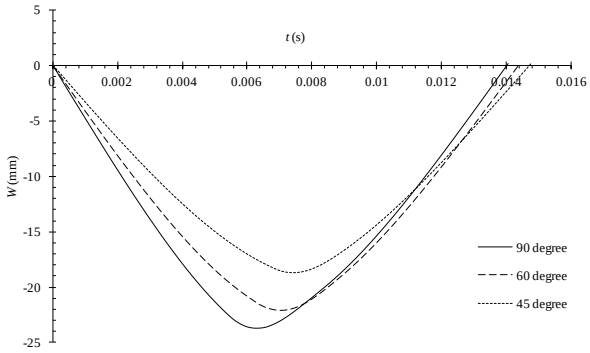

Fig.16
Transverse displacement of 0° composite beam for different angle of impact.

5 CONCLUSIONS

In this paper, the behavior of a beam in the face of impact of a rigid mass is investigated. The model chosen for the beam is Timoshenko's beam model. The collision is of an elastic type and due to the small size of the rigid mass, the pressures and forces created around the area of impact point that are considered in the Hertz Contact Law are ignored. The obtained equations are solved using numerical methods for a multi-layer composite beam. The layers have different angles from the longitudinal axis of the beam. By performing the project, the following results are obtained.

1. As the angle of principle axis of layers increases, the contact force between particle and beam increases.
2. As the angle of principle axis increases, the transverse displacement of beam increases.
3. As the number of layers increases, the transverse displacement and the duration of the collision increases.
4. For the composite beam of four layers whose angles of the layers are [50/30/ 30/50], the stresses and forces formed in the beam are the lowest and after that the [45/-45/-45/45] and [0/90/90/0] beam have lower stresses. The zero-degree angle beams have the highest stress.
5. As the initial speed of the rigid particle increases, the amount of displacement increases. But this increase does not have much effect on the contact time of a rigid particle with a composite beam.
6. Increasing the impact mass causes increased transverse displacement and contact time of the impact.
7. By comparing the impact on a graphite/ epoxy beam with an aluminum beam, it is determined that the stresses and forces in zero-degree graphite / epoxy beam and [090/90/0] beam are greater than the aluminum beam. Also, the stresses in the [45/-45/-45/45] composite beam are less than the stresses in aluminum beam. Also, the separation time of the particle from the beam for the [45/-45 /-45/45] graphite / epoxy beam is much greater than the aluminum beam.
8. When the particle hits on beam vertically (θ = 90), more transverse and axial displacement are created in the beam.

APPENDIX

The variation of Eq. (8) is written as follows:

$$\delta T = \rho b \int_0^L \int_{-\frac{h}{2}}^{\frac{h}{2}} [\dot{u}(x,t)\delta\dot{u}(x,t) + z\dot{u}(x,t)\delta\dot{\varphi}(x,t) + z\,\dot{\varphi}(x,t)\delta\dot{u}(x,t) + z^2\dot{\varphi}(x,t)\delta\dot{\varphi}(x,t) \tag{A.1}$$

$$+\dot{w}\left(x,t\right)\delta\dot{w}\left(x,t\right)]dzdx+M\left[\dot{u}\left(L,t\right)\delta\dot{u}\left(L,t\right)+\dot{w}\left(L,t\right)\delta\dot{w}\left(L,t\right)+\frac{h}{2}\dot{u}\left(L,t\right)\delta\dot{\varphi}\left(L,t\right)+\frac{h}{2}\dot{\varphi}\left(L,t\right)\delta\dot{u}\left(L,t\right)$$
$$+\frac{1}{4}h^2\dot{\varphi}\left(L,t\right)\delta\dot{\varphi}\left(L,t\right)] \tag{A.1}$$

The integration of Eq. (8) respect to z is written as follows:

$$\delta T=\rho b\int_0^L[h\dot{u}\left(x,t\right)\delta\dot{u}\left(x,t\right)+\frac{h^3}{12}\dot{\varphi}\left(x,t\right)\delta\dot{\varphi}\left(x,t\right)+h\dot{w}\left(x,t\right)\delta\dot{w}\left(x,t\right)]dx+M\left[\dot{u}\left(L,t\right)\delta\dot{u}\left(L,t\right)\right.$$
$$\left.+\dot{w}\left(L,t\right)\delta\dot{w}\left(L,t\right)+\frac{h}{2}\dot{u}\left(L,t\right)\delta\dot{\varphi}\left(L,t\right)+\frac{h}{2}\dot{\varphi}\left(L,t\right)\delta\dot{u}\left(L,t\right)+\frac{1}{4}h^2\dot{\varphi}\left(L,t\right)\delta\dot{\varphi}\left(L,t\right)\right] \tag{A.2}$$

The Eq. (8) after integrating respect to time and using integrate by parts is simplified as follows with the assumption $\delta\dot{X}\left(x,t_0\right)=\delta\dot{X}\left(x,t_1\right)=0$:

$$\int_{t_0}^{t_1}\delta T dt=-\rho b\int_{t_0}^{t_1}\int_0^L\left[h\ddot{u}\left(x,t\right)\delta u\left(x,t\right)+\frac{h^3}{12}\ddot{\varphi}\left(x,t\right)\delta\varphi\left(x,t\right)+h\ddot{w}\left(x,t\right)\delta w\left(x,t\right)\right]dtdx$$
$$-\int_{t_0}^{t_1}[M\left[\ddot{u}\left(L,t\right)\delta u\left(L,t\right)+\ddot{w}\left(L,t\right)\delta w\left(L,t\right)+\frac{h}{2}\ddot{u}\left(L,t\right)\delta\varphi\left(L,t\right)+\frac{h}{2}\ddot{\varphi}\left(L,t\right)\delta u\left(L,t\right)\right. \tag{A.3}$$
$$\left.+\frac{1}{4}h^2\ddot{\varphi}\left(L,t\right)\delta\varphi\left(L,t\right)\right]]dt$$

The variation of Eq. (10) is obtained as follows:

$$\delta U=\frac{b}{2}\int_0^L\int_{-\frac{h}{2}}^{\frac{h}{2}}[\tilde{C}_{55}k\left(2\varphi\delta\varphi+2\frac{\partial w}{\partial x}\frac{\partial\delta w}{\partial x}+2\varphi\frac{\partial\delta w}{\partial x}+2\frac{\partial w}{\partial x}\delta\varphi\right)+\tilde{C}_{11}(2\frac{\partial u}{\partial x}\frac{\partial\delta u}{\partial x}+\left(\frac{\partial w}{\partial x}\right)^3\frac{\partial\delta w}{\partial x}$$
$$+2z^2\frac{\partial\varphi}{\partial x}\frac{\partial\delta\varphi}{\partial x}+2\frac{\partial u}{\partial x}\frac{\partial w}{\partial x}\frac{\partial\delta w}{\partial x}+\left(\frac{\partial w}{\partial x}\right)^2\frac{\partial\delta u}{\partial x}+2z\frac{\partial\varphi}{\partial x}\frac{\partial w}{\partial x}\frac{\partial\delta w}{\partial x}+z\left(\frac{\partial w}{\partial x}\right)^2\frac{\partial\delta\varphi}{\partial x}+2z\frac{\partial u}{\partial x}\frac{\partial\delta\varphi}{\partial x} \tag{A.4}$$
$$+2z\frac{\partial\varphi}{\partial x}\frac{\partial\delta u}{\partial x})]dzdx+mg\delta w\left(L,t\right)$$

After integrating respect to h, the Eq. (11) is simplified as follows:

$$\delta U=b\int_0^L[A_{55}k\left(\varphi\delta\varphi+\frac{\partial w}{\partial x}\frac{\partial\delta w}{\partial x}+\varphi\frac{\partial\delta w}{\partial x}+\frac{\partial w}{\partial x}\delta\varphi\right)+A_{11}(\frac{\partial u}{\partial x}\frac{\partial\delta u}{\partial x}+\frac{1}{2}\left(\frac{\partial w}{\partial x}\right)^2\frac{\partial\delta u}{\partial x}+\frac{1}{2}\left(\frac{\partial w}{\partial x}\right)^3\frac{\partial\delta w}{\partial x}$$
$$+\frac{\partial u}{\partial x}\frac{\partial w}{\partial x}\frac{\partial\delta w}{\partial x})+B_{11}\left(\frac{\partial\varphi}{\partial x}\frac{\partial w}{\partial x}\frac{\partial\delta w}{\partial x}+\frac{1}{2}\left(\frac{\partial w}{\partial x}\right)^2\frac{\partial\delta\varphi}{\partial x}+\frac{\partial u}{\partial x}\frac{\partial\delta\varphi}{\partial x}+\frac{\partial\varphi}{\partial x}\frac{\partial\delta u}{\partial x}\right)+D_{11}\frac{\partial\varphi}{\partial x}\frac{\partial\delta\varphi}{\partial x}]dx+mg\delta w\left(L,t\right) \tag{A.5}$$

By using integration by parts, the Eq. (11) is simplified as follows:

$$\delta U=b\int_0^L[A_{55}k\left(\varphi\delta\varphi+\frac{\partial w}{\partial x}\delta\varphi-\frac{\partial\varphi}{\partial x}\delta w-\frac{\partial^2 w}{\partial x^2}\delta w\right)+A_{11}(-\frac{\partial^2 u}{\partial x^2}\delta u-\frac{\partial w}{\partial x}\frac{\partial^2 w}{\partial x^2}\delta u-\frac{\partial^2 u}{\partial x^2}\frac{\partial w}{\partial x}\delta w-\frac{\partial u}{\partial x}\frac{\partial^2 w}{\partial x^2}\delta w \tag{A.6}$$

$$-\frac{3}{2}\frac{\partial^2 w}{\partial x^2}\left(\frac{\partial w}{\partial x}\right)^2\delta w)+B_{11}\left(-\frac{\partial^2\varphi}{\partial x^2}\delta u-\frac{\partial^2 u}{\partial x^2}\delta u-\frac{\partial w}{\partial x}\frac{\partial^2 w}{\partial x^2}\delta u\right)-D_{11}\frac{\partial^2\varphi}{\partial x^2}\delta\varphi\Big]dx+\Big[A_{55}k\left(\frac{\partial w}{\partial x}\delta w+\varphi\delta w\right)\Big]$$
$$+A_{11}\left(\frac{\partial u}{\partial x}\delta u+\frac{1}{2}\left(\frac{\partial w}{\partial x}\right)^2\delta u+\frac{1}{2}\left(\frac{\partial w}{\partial x}\right)^3\delta w+\frac{\partial u}{\partial x}\frac{\partial w}{\partial x}\delta w\right)+B_{11}\left(\frac{\partial\varphi}{\partial x}\frac{\partial w}{\partial x}\delta w+\frac{1}{2}\left(\frac{\partial w}{\partial x}\right)^2\delta\varphi+\frac{\partial u}{\partial x}\delta\varphi+\frac{\partial\varphi}{\partial x}\delta u\right)$$
$$+D_{11}\frac{\partial\varphi}{\partial x}\delta\varphi]\Big|_0^L+mg\,\delta w\,(L,t)$$

By placing the Eq. (11) and (12) in Eq. (5), the Hamilton's principle relation is obtained as follows:

$$\int_{t_0}^{t_1}\int_0^L(\Big[-\rho hb\frac{\partial^2 u}{\partial t^2}+bA_{11}\left(\frac{\partial^2 u}{\partial x^2}+\frac{\partial w}{\partial x}\frac{\partial^2 w}{\partial x^2}\right)+bB_{11}\frac{\partial^2\varphi}{\partial x^2}\Big]\delta u(x,t)+[bD_{11}\frac{\partial^2\varphi}{\partial x^2}+bB_{11}\left(\frac{\partial^2 u}{\partial x^2}+\frac{\partial w}{\partial x}\frac{\partial^2 w}{\partial x^2}\right)$$
$$-bA_{55}k\left(\varphi+\frac{\partial w}{\partial x}\right)-\frac{1}{12}\rho bh^3\frac{\partial^2\varphi}{\partial t^2}]\delta\varphi(x,t)+[A_{55}bk\left(\frac{\partial\varphi}{\partial x}+\frac{\partial^2 w}{\partial x^2}\right)+bB_{11}\left(\frac{\partial^2\varphi}{\partial x^2}\frac{\partial w}{\partial x}+\frac{\partial\varphi}{\partial x}\frac{\partial^2 w}{\partial x^2}\right)$$
$$+bA_{11}\left(\frac{\partial^2 u}{\partial x^2}\frac{\partial w}{\partial x}+\frac{\partial u}{\partial x}\frac{\partial^2 w}{\partial x^2}+\frac{3}{2}\frac{\partial^2 w}{\partial x^2}\left(\frac{\partial w}{\partial x}\right)^2\right)-\rho bh\frac{\partial^2 w}{\partial t^2}]\delta w\,(x,t))dx+\int_{t_0}^{t_1}[(-bA_{11}\left(\frac{\partial u}{\partial x}+\frac{1}{2}\left(\frac{\partial w}{\partial x}\right)^2\right)$$
$$-bB_{11}\frac{\partial\varphi}{\partial x}-M\left(\frac{\partial^2 u}{\partial t^2}+\frac{h}{2}\frac{\partial^2\phi}{\partial t^2}\right))\delta u(x,t)\Big|_0^L+(-bD_{11}\frac{\partial\phi}{\partial x}-bB_{11}\left(\frac{\partial u}{\partial x}+\frac{1}{2}\left(\frac{\partial w}{\partial x}\right)^2\right)-\frac{Mh}{2}(\frac{\partial^2 u}{\partial t^2} \tag{A.7}$$
$$+\frac{h}{2}\frac{\partial^2\phi}{\partial t^2}))\delta\varphi(x,t)\Big|_0^L+(-bA_{55}k\left(\phi+\frac{\partial w}{\partial x}\right)-bA_{11}\left(\frac{\partial u}{\partial x}\frac{\partial w}{\partial x}+\frac{1}{2}\left(\frac{\partial w}{\partial x}\right)^3\right)-bB_{11}\frac{\partial\varphi}{\partial x}\frac{\partial w}{\partial x}$$
$$-M\frac{\partial^2 w}{\partial t^2})\delta w\,(x,t)\Big|_0^L-Mg\,\delta w\,(L,t)]dt=0$$

Finally the motion equation and boundary conditions are obtained as follows:

$$\delta u(x,t)=0\qquad A_{11}\left(\frac{\partial^2 u}{\partial x^2}+\frac{\partial w}{\partial x}\frac{\partial^2 w}{\partial x^2}\right)+B_{11}\frac{\partial^2\varphi}{\partial x^2}=\rho h\frac{\partial^2 u}{\partial t^2}$$
$$\delta\varphi(x,t)=0\qquad D_{11}\frac{\partial^2\varphi}{\partial x^2}+B_{11}\left(\frac{\partial^2 u}{\partial x^2}+\frac{\partial w}{\partial x}\frac{\partial^2 w}{\partial x^2}\right)-A_{55}k\left(\varphi+\frac{\partial w}{\partial x}\right)=\frac{1}{12}\rho h^3\frac{\partial^2\varphi}{\partial t^2} \tag{A.8}$$
$$\delta w\,(x,t)=0\qquad A_{55}k\left(\frac{\partial\varphi}{\partial x}+\frac{\partial^2 w}{\partial x^2}\right)+B_{11}\left(\frac{\partial^2\varphi}{\partial x^2}\frac{\partial w}{\partial x}+\frac{\partial\varphi}{\partial x}\frac{\partial^2 w}{\partial x^2}\right)+A_{11}\left(\frac{\partial^2 u}{\partial x^2}\frac{\partial w}{\partial x}+\frac{\partial u}{\partial x}\frac{\partial^2 w}{\partial x^2}+\frac{3}{2}\frac{\partial^2 w}{\partial x^2}\left(\frac{\partial w}{\partial x}\right)^2\right)=\rho h\frac{\partial^2 w}{\partial t^2}$$

Boundary conditions:

$$\begin{aligned}&\delta u(0,t)=0 && u(0,t)=0\\ &\delta\varphi(0,t)=0 && \varphi(0,t)=0\\ &\delta w\,(0,t)=0 && w\,(0,t)=0\end{aligned} \tag{A.9}$$

$$\begin{aligned}
&\delta u\left(L,t\right)=0 \qquad A_{11}\left(\frac{\partial u}{\partial x}+\frac{1}{2}\left(\frac{\partial w}{\partial x}\right)^2\right)+B_{11}\frac{\partial \varphi}{\partial x}+\frac{M}{b}\left(\frac{\partial^2 u}{\partial t^2}+\frac{h}{2}\frac{\partial^2 \phi}{\partial t^2}\right)=0\\
&\delta \varphi\left(L,t\right)=0 \qquad D_{11}\frac{\partial \phi}{\partial x}+B_{11}\left(\frac{\partial u}{\partial x}+\frac{1}{2}\left(\frac{\partial w}{\partial x}\right)^2\right)+\frac{Mh}{2b}\left(\frac{\partial^2 u}{\partial t^2}+\frac{h}{2}\frac{\partial^2 \phi}{\partial t^2}\right)=0\\
&\delta w\left(L,t\right)=0 \qquad A_{55}k\left(\phi+\frac{\partial w}{\partial x}\right)+A_{11}\left(\frac{\partial u}{\partial x}\frac{\partial w}{\partial x}+\frac{1}{2}\left(\frac{\partial w}{\partial x}\right)^3\right)+B_{11}\frac{\partial \varphi}{\partial x}\frac{\partial w}{\partial x}+\frac{M}{b}\left(g+\frac{\partial^2 w}{\partial t^2}\right)=0
\end{aligned} \tag{A.10}$$

The motion equations after applying numerical methods ("n" is the number of time step and it begins from zero):

$$\begin{aligned}
&A_{11}\left(\sum_{j=1}^{N}c_{ij}^{(2)}u_j{}^{(n+1)}+\sum_{j=1}^{N}c_{ij}^{(1)}w_j{}^{(n+1)}\sum_{k=1}^{N}c_{ik}^{(2)}w_k{}^{(n+1)}\right)+B_{11}\sum_{j=1}^{N}c_{ij}^{(2)}\varphi_j{}^{(n+1)}-\frac{\rho h}{\beta\Delta t^2}u_i{}^{(n+1)}=\rho h[(1-\frac{1}{2\beta})\ddot{u}_i{}^{(n)}-\frac{1}{\beta\Delta t^2}u_i{}^{(n)}\\
&-\frac{1}{\beta\Delta t}\dot{u}_i{}^{(n)}] \quad ,\ i=2,3,\ldots,N-1
\end{aligned} \tag{A.11}$$

$$\begin{aligned}
&D_{11}\sum_{j=1}^{N}c_{ij}^{(2)}\varphi_j{}^{(n+1)}+B_{11}\left(\sum_{j=1}^{N}c_{ij}^{(2)}u_j{}^{(n+1)}+\sum_{j=1}^{N}c_{ij}^{(1)}w_j{}^{(n+1)}\sum_{k=1}^{N}c_{ik}^{(2)}w_k{}^{(n+1)}\right)-A_{55}k\left(\varphi_i{}^{(n+1)}+\sum_{j=1}^{N}c_{ij}^{(1)}w_j{}^{(n+1)}\right)-\frac{\rho h^3}{\beta\Delta t^2}\varphi_i{}^{(n+1)}\\
&=\frac{1}{12}\rho h^3\left[\left(1-\frac{1}{2\beta}\right)\ddot{\varphi}_i{}^{(n)}-\frac{1}{\beta\Delta t^2}\varphi_i{}^{(n)}-\frac{1}{\beta\Delta t}\dot{\varphi}_i{}^{(n)}\right] \quad ,\ i=2,3,\ldots,N-1
\end{aligned} \tag{A.12}$$

$$\begin{aligned}
&A_{55}k\left(\sum_{j=1}^{N}c_{ij}^{(1)}\varphi_j{}^{(n+1)}+\sum_{j=1}^{N}c_{ij}^{(2)}w_j{}^{(n+1)}\right)+B_{11}\left(\sum_{j=1}^{N}c_{ij}^{(2)}\varphi_j{}^{(n+1)}\sum_{k=1}^{N}c_{ik}^{(1)}w_k{}^{(n+1)}+\sum_{j=1}^{N}c_{ij}^{(1)}\varphi_j{}^{(n+1)}\sum_{k=1}^{N}c_{ik}^{(2)}w_k{}^{(n+1)}\right)\\
&+A_{11}\left(\sum_{j=1}^{N}c_{ij}^{(2)}u_j{}^{(n+1)}\sum_{k=1}^{N}c_{ik}^{(1)}w_k{}^{(n+1)}+\sum_{j=1}^{N}c_{ij}^{(1)}u_j\sum_{k=1}^{N}c_{ik}^{(2)}w_k+\frac{3}{2}\sum_{j=1}^{N}c_{ij}^{(2)}w_j\sum_{k=1}^{N}c_{ik}^{(1)}w_k\sum_{t=1}^{N}c_{it}^{(1)}w_t\right)\\
&-\frac{\rho h}{\beta\Delta t^2}w_i{}^{(n+1)}=\rho h\left[\left(1-\frac{1}{2\beta}\right)\ddot{w}_i{}^{(n)}-\frac{1}{\beta\Delta t^2}w_i{}^{(n)}-\frac{1}{\beta\Delta t}\dot{w}_i{}^{(n)}\right] \quad ,\ i=2,3,\ldots,N-1
\end{aligned} \tag{A.13}$$

The boundary conditions:

$$x=0:\ \ u=\varphi=w=0 \tag{A.14}$$

$$\begin{aligned}
&x=L:\\
&A_{11}\left(\sum_{j=1}^{N}c_{Nj}^{(1)}u_j{}^{(n+1)}+\frac{1}{2}\sum_{j=1}^{N}c_{Nj}^{(1)}w_j{}^{(n+1)}\sum_{k=1}^{N}c_{Nk}^{(1)}w_k{}^{(n+1)}\right)+B_{11}\sum_{j=1}^{N}c_{Nj}^{(1)}\varphi_j{}^{(n+1)}+\frac{M}{b}([\frac{u_i{}^{(n+1)}}{\beta\Delta t^2}+\left(1-\frac{1}{2\beta}\right)\ddot{u}_N{}^{(n)}-\frac{1}{\beta\Delta t^2}u_N{}^{(n)}\\
&-\frac{1}{\beta\Delta t}\dot{u}_N{}^{(n)}]+\frac{h}{2}\left[\frac{\varphi_i{}^{(n+1)}}{\beta\Delta t^2}+\left(1-\frac{1}{2\beta}\right)\ddot{\varphi}_N{}^{(n)}-\frac{1}{\beta\Delta t^2}\varphi_N{}^{(n)}-\frac{1}{\beta\Delta t}\dot{\varphi}_N{}^{(n)}\right])=0
\end{aligned} \tag{A.15}$$

$$\begin{aligned}
&D_{11}\sum_{j=1}^{N}c_{Nj}^{(1)}\varphi_j{}^{(n+1)}+B_{11}\left(\sum_{j=1}^{N}c_{Nj}^{(1)}u_j{}^{(n+1)}+\frac{1}{2}\sum_{j=1}^{N}c_{Nj}^{(1)}w_j{}^{(n+1)}\sum_{k=1}^{N}c_{Nk}^{(1)}w_k{}^{(n+1)}\right)+\frac{Mh}{2b}([\frac{u_i{}^{(n+1)}}{\beta\Delta t^2}+\left(1-\frac{1}{2\beta}\right)\ddot{u}_N{}^{(n)}-\frac{1}{\beta\Delta t^2}u_N{}^{(n)}\\
&-\frac{1}{\beta\Delta t}\dot{u}_N{}^{(n)}]+\frac{h}{2}[\frac{\varphi_i{}^{(n+1)}}{\beta\Delta t^2}+\left(1-\frac{1}{2\beta}\right)\ddot{\varphi}_N{}^{(n)}-\frac{1}{\beta\Delta t^2}\varphi_N{}^{(n)}-\frac{1}{\beta\Delta t}\dot{\varphi}_N{}^{(n)}])=0
\end{aligned} \tag{A.16}$$

$$A_{55}k\left(\varphi_N{}^{(n+1)}+\sum_{j=1}^{N}c_{Nj}^{(1)}w_j{}^{(n+1)}\right)+A_{11}\left(\sum_{j=1}^{N}c_{Nj}^{(1)}u_j{}^{(n+1)}\sum_{j=1}^{N}c_{Nj}^{(1)}w_j{}^{(n+1)}+\frac{1}{2}\sum_{j=1}^{N}c_{Nj}^{(1)}w_j{}^{(n+1)}\sum_{k=1}^{N}c_{Nk}^{(1)}w_k{}^{(n+1)}\sum_{t=1}^{N}c_{Nt}^{(1)}w_t{}^{(n+1)}\right)$$
$$+B_{11}\sum_{j=1}^{N}c_{Nj}^{(1)}\varphi_j{}^{(n+1)}\sum_{j=1}^{N}c_{Nj}^{(1)}w_j{}^{(n+1)}+\frac{M}{b}(g+[\frac{w_i{}^{(n+1)}}{\beta\Delta t^2}+\left(1-\frac{1}{2\beta}\right)\ddot{w}_N{}^{(n)}-\frac{1}{\beta\Delta t^2}w_N{}^{(n)}-\frac{1}{\beta\Delta t}\dot{w}_N{}^{(n)}])=0 \tag{A.17}$$

The contact force is as follows:

$$V=A_{55}k\left(\varphi_N{}^{(n+1)}+\sum_{j=1}^{N}c_{Nj}^{(1)}w_j{}^{(n+1)}\right)+A_{11}\left(\sum_{j=1}^{N}c_{Nj}^{(1)}u_j{}^{(n+1)}\sum_{k=1}^{N}c_{Nk}^{(1)}w_k{}^{(n+1)}+\frac{1}{2}\sum_{j=1}^{N}c_{Nj}^{(1)}w_j{}^{(n+1)}\sum_{k=1}^{N}c_{Nk}^{(1)}w_k{}^{(n+1)}\sum_{t=1}^{N}c_{Nt}^{(1)}w_t{}^{(n+1)}\right)$$
$$+B_{11}\sum_{j=1}^{N}c_{Nj}^{(1)}\varphi_j{}^{(n+1)}\sum_{k=1}^{N}c_{Nk}^{(1)}w_k{}^{(n+1)} \tag{A.18}$$

Motion equations for aluminum beam:

$$\frac{\partial^2 u}{\partial x^2}+\frac{\partial w}{\partial x}\frac{\partial^2 w}{\partial x^2}=\frac{\rho}{E}\frac{\partial^2 u}{\partial t^2} \tag{A.19}$$

$$\frac{\partial^2\varphi}{\partial x^2}-\frac{6k}{(1+\nu)h^2}\left(\varphi+\frac{\partial w}{\partial x}\right)=\frac{\rho}{E}\frac{\partial^2\varphi}{\partial t^2} \tag{A.20}$$

$$\frac{k}{2(1+\nu)}\left(\frac{\partial\varphi}{\partial x}+\frac{\partial^2 w}{\partial x^2}\right)+\frac{\partial^2 u}{\partial x^2}\frac{\partial w}{\partial x}+\frac{\partial u}{\partial x}\frac{\partial^2 w}{\partial x^2}+\frac{3}{2}\frac{\partial^2 w}{\partial x^2}\left(\frac{\partial w}{\partial x}\right)^2=\frac{\rho}{E}\frac{\partial^2 w}{\partial t^2} \tag{A.21}$$

Boundary conditions:

$$x=0:\quad u=\varphi=w=0 \tag{A.22}$$

$$x=L:$$
$$\frac{\partial u}{\partial x}+\frac{1}{2}\left(\frac{\partial w}{\partial x}\right)^2+\frac{M}{Eb}\left(\frac{\partial^2 u}{\partial t^2}+\frac{h}{2}\frac{\partial^2\phi}{\partial t^2}\right)=0 \tag{A.23}$$

$$\frac{\partial\phi}{\partial x}+\frac{Mh}{2Eb}\left(\frac{\partial^2 u}{\partial t^2}+\frac{h}{2}\frac{\partial^2\phi}{\partial t^2}\right)=0 \tag{A.24}$$

$$\frac{Ebhk}{2(1+\nu)}\left(\phi+\frac{\partial w}{\partial x}\right)+Ebh\left(\frac{\partial u}{\partial x}\frac{\partial w}{\partial x}+\frac{1}{2}\left(\frac{\partial w}{\partial x}\right)^3\right)+\frac{M}{b}\left(g+\frac{\partial^2 w}{\partial t^2}\right)=0 \tag{A.25}$$

REFERENCES

[1] Abrate S., 2011, *Impact Engineering of Composite Structures*, Springer Science & Business Media.
[2] Zener C., 1941, The intrinsic inelasticity of large plates, *Physical Review* **59**(8): 669-673.
[3] Müller P., Böttcher R., Russell A., Trüe M., Aman S., Tomas J., 2016, Contact time at impact of spheres on large thin plates, *Advanced Powder Technology* **27**(4): 1233-1243 .

[4] Boettcher R., Russell A., Mueller P., 2017, Energy dissipation during impacts of spheres on plates: Investigation of developing elastic flexural waves, *International Journal of Solids and Structures* **106**: 229-239.
[5] Hunter S., 1957, Energy absorbed by elastic waves during impact, *Journal of the Mechanics and Physics of Solids* **5**(3): 162-171.
[6] Reed J., 1985, Energy losses due to elastic wave propagation during an elastic impact, *Journal of Physics D: Applied Physics* **18**(12): 2329.
[7] Weir G., Tallon S., 2005, The coefficient of restitution for normal incident, low velocity particle impacts, *Chemical Engineering Science* **60**(13): 3637-3647.
[8] Kelly J. M., 1967, The impact of a mass on a beam, *International Journal of Solids and Structures* **3**(2): 191-196.
[9] Sun C., Huang S., 1975, Transverse impact problems by higher order beam finite element, *Computers & Structures* **5** (5-6): 297-303.
[10] Yufeng X., Yuansong Q., Dechao Z., Guojiang S., 2002, Elastic impact on finite Timoshenko beam, *Acta Mechanica Sinica* **18**(3): 252-263.
[11] Kiani Y., Sadighi M., Salami S. J., Eslami M., 2013, Low velocity impact response of thick FGM beams with general boundary conditions in thermal field, *Composite Structures* **104**: 293-303.
[12] Rezvanian M., Baghestani A., Pazhooh M. D., Fariborz S., 2015, Off-center impact of an elastic column by a rigid mass, *Mechanics Research Communications* **63**: 21-25.
[13] Ghatreh Samani K., Fotuhi A. R., Shafiei A. R., 2017, Analysis of composite beam, having initial geometric imperfection, subjected to off-center impact, *Modares Mechanical Engineering* **17**(5): 185-192.
[14] Singh H., Mahajan P., 2016, Analytical modeling of low velocity large mass impact on composite plate including damage evolution, *Composite Structures* **149**: 79-92.
[15] Shivakumar K. N., Elber W., Illg W., 1985, Prediction of impact force and duration due to low-velocity impact on circular composite laminates, *Journal of Applied Mechanics* **52**(3): 674-680.
[16] Lam K., Sathiyamoorthy T., 1999, Response of composite beam under low-velocity impact of multiple masses, *Composite Structures* **44**(2-3): 205-220.
[17] Ugural A. C., 2009, *Stresses in Beams, Plates, and Shells*, CRC Press.
[18] Elshafei M. A., 2013, FE Modeling and analysis of isotropic and orthotropic beams using first order shear deformation theory, *Materials Sciences and Applications* **4**(01): 77.
[19] Reddy J. N., 2004, *Mechanics of Laminated Composite Plates and Shells: Theory and Analysis*, CRC press.
[20] Newmark N. M., 1959, A method of computation for structural dynamics, *Journal of the Engineering Mechanics Division* **85**(3): 67-94.
[21] Hilber H. M., Hughes T. J., Taylor R. L., 1977, Improved numerical dissipation for time integration algorithms in structural dynamics, *Earthquake Engineering & Structural Dynamics* **5**(3): 283-292.
[22] Shu C., Wang C., 1999, Treatment of mixed and nonuniform boundary conditions in GDQ vibration analysis of rectangular plates, *Engineering Structures* **21**(2): 125-134.
[23] Reddy J., 2004, *An Introduction to Nonlinear Finite Element Analysis*, United State, Oxford.